Robust Au—Ag—Au Bimetallic Atom-Scale Junctions Fabricated by Self-Limited Ag Electrodeposition at Au Nanogaps

Tai-Wei Hwang[†] and Paul W. Bohn[†,‡,*]

[†]Department of Chemical and Biomolecular Engineering and [‡]Department of Chemistry and Biochemistry, University of Notre Dame, Notre Dame, Indiana 46556, United States

ABSTRACT Atom-scale junctions (ASJs) exhibit quantum conductance behavior and have potential both for fundamental studies of adsorbate-mediated conductance in mesoscopic conductors and as chemical sensors. Electrochemically fabricated ASJs, in particular, show the stability needed for molecular detection applications. However, achieving physically robust ASJs at high yield is a challenge because it is difficult to control the direction and kinetics of metal deposition. In this work, a novel electrochemical approach is reported, in which Au—Ag—Au bimetallic ASJs are reproducibly fabricated from an initially prepared Au nanogap by sequential overgrowth and self-limited thinning. Applying a potential across specially prepared Au nanoelectrodes in the presence of aqueous Ag(I) leads to preferential galvanic reactions resulting in the deposition of Ag and the formation of an atom-scale junction between the electrodes. An external resistor is added in series with the ASJ to control self-termination, and adjusting solution chemical potential (concentration) is used to mediate self-thinning of junctions. The result is long-lived, mechanically stable ASJs that, unlike previous constructions, are stable in flowing solution, as well as to changes in solution media. These bimetallic ASJs exhibit a number of behaviors characteristic of quantum structures, including long-lived fractional conductance states, that are interpreted to arise from two or more quantized ASJs in series.

KEYWORDS: atom-scale junction · nanowire · electrochemical nanofabrication · fractional conductance · self-termination · bimetallic

Atom-scale junctions (ASJs) have garnered a great deal of interest both for their potential as chemical sensors and for their application to fundamental studies of conductance in mesoscopic structures.[1−12] The defining characteristic of metallic ASJs is quantized conductance. Classically, the conductance of a wire is given by $G = \sigma A/L$, where σ is the conductivity, and L and A are the length and the cross-sectional area of the wire, respectively. However, the physical dimensions of ASJs approach the Fermi wavelength of electron in the material, resulting in quantized conductance, given by

$$G = G_0 \sum_i^N T_i \qquad (1)$$

where $G_0 = 2e^2/h = 77.4\ \mu S = 1/(12.9\ k\Omega)$ is the conductance quantum, e is the electron charge, h is Planck's constant, and T_i is the transmission probability of the ith channel. For an ideal ASJ, $T_i = 1$ and $G = NG_0$, resulting in ballistic transport, a phenomenon observed when the wire length is much smaller than both the mean free path and phase relaxation length of the electron.[13,14] Due to their unusual characteristics, ASJs are of interest in several lab-on-a-chip applications such as atomic-scale transistors[15,16] and multiatom relays.[8] Moreover, the large conductance change due to molecular adsorption in the ballistic transport regime makes ASJs sensitive to molecular adsorption.[6,17−19]

To date, several approaches have been reported to fabricate ASJs. Mechanical methods such as mechanically controllable break junctions, which are formed by bending a thin metal wire with a piezoactuator,[20] and using STM tips to create nanocontacts by sweeping away from the substrate surface[19,21] are widely used. However, ASJs fabricated by mechanical methods typically display short lifetimes and impose rigid constraints on positioning of experimental components. On the other hand, electrochemical ASJ fabrication can be controlled electronically,[12,16,17,22−26] and ASJs have been fabricated from many different metals, including Au,[12,17,22] Ag,[23,24] Cu,[23−25] and Pb.[16,23] ASJs fabricated by electrochemical methods are typically more stable than those fabricated by mechanical methods, displaying lifetimes of tens of seconds to hours at room temperature.

Several different electrochemical fabrication protocols have been developed.

* Address correspondence to pbohn@nd.edu.

Received for review September 2, 2011 and accepted September 17, 2011.

Published online September 17, 2011
10.1021/nn203404k

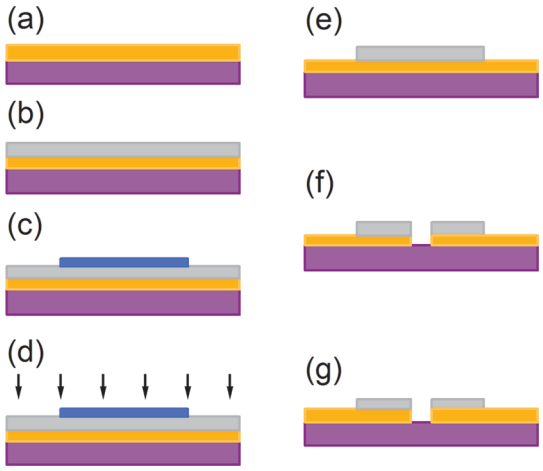

Figure 1. Fabrication of template. (a) Au thin film microbridge defined photolithographically; (b) PECVD deposition of SiN_x; (c) thermal evaporation of 30 nm Cr mask; (d) reactive ion etching of exposed SiN_x; (e) Cr removal with CR-4 etchant; (f) direct-write patterning of electrodes by focused ion beam milling; (g) rinse in 1:1 (v/v) aqueous HNO_3.

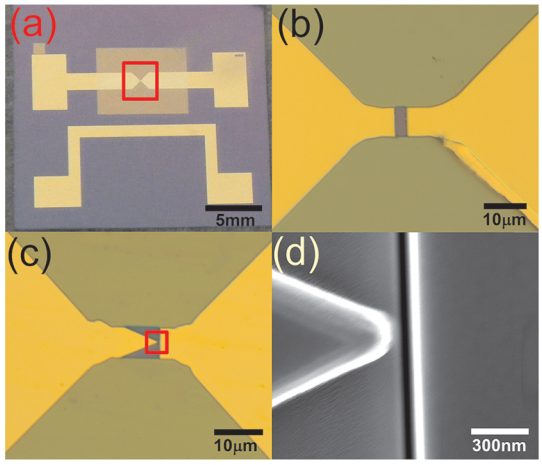

Figure 2. (a) Macroscale top view of the sample template. The highlighted area is the Au microbridge which is milled by FIB into two different electrode designs. The bottom Au stripe functions as a quasi-reference/counter electrode (QR/CE) for electrochemical studies. (b) Electrode design for electrochemical characterization. One electrode is used as the working electrode (WE), coupled with the QR/CE stripe to form a two-electrode system. (c) Optical micrograph showing the tip and anvil electrode design for ASJ fabrication. (d) Scanning electron micrograph (SEM) exploded view of the highlighted area in (c). The distance between the end of the tip electrode and the flat electrode is 115 nm.

The most commonly used approach begins with two electrodes separated by a nanometer-scale gap that are used as working electrodes (WEs) and are coupled with counter (CE) and reference (RE) electrodes in a three-electrode cell.[26−28] However, this approach results in metal being deposited isotropically, with no directional bias to close the gap and form a junction. In addition, the kinetics of deposition are hard to control. Directional electrodeposition, a process first used to fabricate ASJs by Boussaad *et al.*,[22] guarantees junction formation with self-termination by simply connecting an external resistor in series with the sample, thereby assuring that the applied potential drops below the deposition range once contact is made. An extension of the electrodeposition approach, employing an open working electrode developed in this laboratory,[24] was successful in slowing the deposition kinetics and achieving excellent control over quantum conductance, but devices prepared this way are susceptible to both mechanical and oxidative damage.

A new electrochemical method of preparing Au−Ag−Au bimetallic ASJs is explored here. Characterizing the electrochemistry of Ag deposition/dissolution in different concentrations at nanoscale electrodes illustrates how deposition potential varies with history of the electrode and how the chemical potential of solution can affect the deposition/dissolution dynamics of Ag at nanoelectrodes. On the basis of these studies, a design starting from a Au microbridge (Figure 1) was used to produce differently shaped electrodes, which were prepared by focused ion beam (FIB) milling (Figure 2). The tip and anvil design (Figure 2c,d) was found to concentrate the electric field and facilitate directional galvanic deposition in the Ag_2SO_4 electrolyte, resulting in highly stable and controllable Au−Ag−Au bimetallic ASJs. This fabrication protocol typically produces junctions that are initially overgrown ($G > 10\ G_0$), but the kinetic overshoot is followed by a self-thinning process controlled by the chemical potential of the Ag^+ in solution and an external ballast resistor. ASJs formed under these conditions typically are thinned to $G \sim G_0$ and remain stable for hundreds of seconds. Furthermore, the back-thinned ASJs are very mechanically robust, being stable under flow and allowing medium changeover from electrolyte solution to air and back to deionized (DI) water. The resulting bimetallic ASJs exhibit a number of behaviors characteristic of quantum structures, including long-lived fractional conductance states, that are interpreted to arise from two or more quantized ASJs in series.

RESULTS AND DISCUSSION

Electrochemical Characterization. It is important to investigate the electrochemical characteristics of the nanogap electrodes, which are prepared as the starting point for ASJ formation, because nanoscale transport dynamics differ significantly from those on longer length scales. Figure 3a shows the two-electrode configuration, employing a single QR/CE, used to acquire cyclic voltammetry (CV) data at a nanoband electrode, and the behavior of the nanoband electrode in 1 mM Ag_2SO_4 is compared to a macroscale Au wire WE in the same solution in Figure 4. Figure 4a shows that the macroscale WE exhibits a Ag deposition peak at ~−0.1 V, while dissolution occurs at ~0.1 V. The behavior is contrasted to that at a nanoscale WE in Figure 4b. Several differences are apparent. Obviously, the nanoelectrode

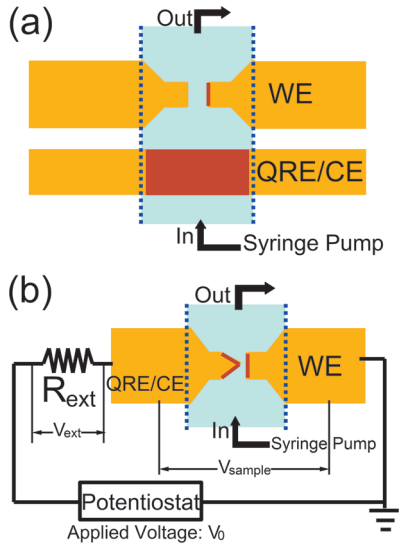

Figure 3. (a) Schematic diagram (top view) of the sample for electrochemical studies. (b) Configuration for electrochemical fabrication of ASJs. A potentiostat is used to apply constant voltage while simultaneously measuring the current to monitor ASJ formation. The red areas indicate the Au surfaces exposed to solution.

current is small (~50 pA) compared to that in Figure 4a, and it is dominated by a capacitive component that is mostly due to the parasitic charging of dielectric materials at the interfaces between gold thin film electrodes and the surrounding SiO_2 and SiN_x dielectrics.[29,30] This assignment is confirmed by running the same CV voltage−time program in the absence of solution (data not shown). In addition, the deposition potential at nanoscale electrodes shifts cathodically in successive cycles, and the deposition is irreversible. Clearly, the surface properties change from cycle-to-cycle. In the first cycle, deposition occurs at a bare Au polycrystalline surface and likely corresponds to underpotential deposition of Ag on polycrystalline Au at relatively anodic potentials.[31,32] Because the solution Ag^+ concentration is relatively high, the opposite potential sweep shows little Ag stripping, and with successive scans, Ag^+ deposition occurs on increasingly bulk-like Ag substrates, consistent with the observed cathodic shift of the deposition peak.

To further explore the reversibility of Ag deposition at nanoscale WEs, different concentrations of Ag_2SO_4 in 0.1 M K_2SO_4 solution were investigated. Figure 5a represents the third CV cycle of seven cycles at different Ag^+ concentrations, while Figure 5b shows all seven cycles at each concentration. The 1, 10, and 100 μM CVs do not show peak deposition currents, but there are inflection points between −0.5 and −0.6 V, approximately where deposition would be expected. As the concentration increases, the reduction currents become more obvious, and a current peak is observed at 1 mM, as in Figure 4b. The oxidation currents, however, do not show the same trend. In the 1 μM CV, a small peak is observed at ~−0.2 V, independent of how many cycles are performed and is most likely related to the dissolution of the first several

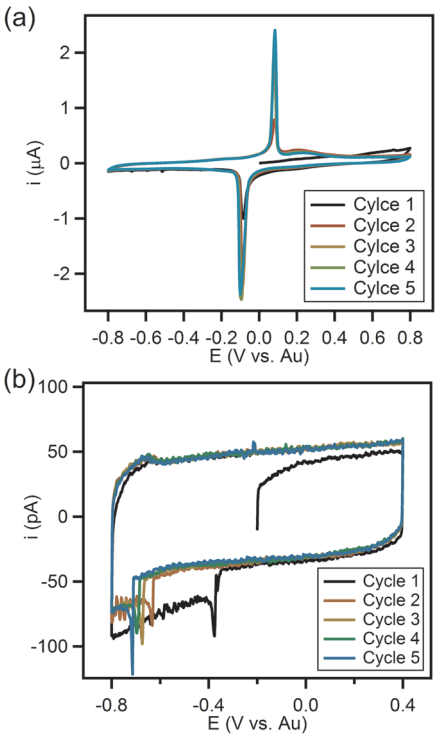

Figure 4. (a) Cyclic voltammetry of macroscale (500 μm diameter) Au electrode in 1 mM Ag_2SO_4/0.1 M K_2SO_4 at a scan rate of 20 mV s^{-1}. Negative current corresponds to reduction (deposition) and positive current to oxidation (dissolution). Scans are 0 V to 0.8 V to −0.8 V to 0 V *vs* Au QR/CE. (b) Cyclic voltammetry obtained under same conditions with a nanoscale WE (100 nm × 6 μm). Scans are −0.2 V to 0.4 V to −0.8 V to −0.2 V *vs* Au film QR/CE.

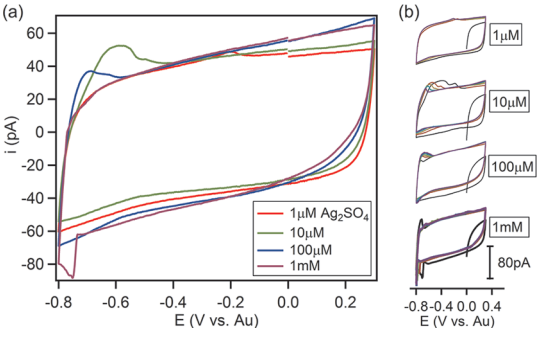

Figure 5. Cyclic voltammetry of Ag_2SO_4 in 0.1 M aqueous K_2SO_4 at a nanoband WE at 20 mV s^{-1} scan rate *vs* Au thin film QR/CE. (a) Third cycle (out of seven) as a function of Ag_2SO_4 concentration. (b) Seven full cycles at concentrations ranging from 1 μM to 1 mM. All scans start at 0 V, scan anodically to 0.2 V, then cathodically to −0.8 V and back to 0 V.

layers of deposited Ag. At 10 μM, the dissolution of Ag is clearly evident; however, as the concentration increases, the dissolution of Ag becomes less favorable as seen in 100 μM CV. At 1 mM, the oxidation current can hardly be observed. This experiment indicates that the chemical potential of Ag in solution affects the reversibility of Ag deposition/dissolution at a nanoscale WE and suggests a means to control the rate of Ag growth during the formation of Au−Ag−Au bimetallic ASJs.

ASJ Fabrication by Self-Limiting Ag Electrodeposition. Figure 2c shows the tip and anvil design for ASJ fabrication. The SiN_x-covered Au microbridge is FIB milled into one sharp and one flat electrode separated typically by 100 to 150 nm, viz. Figure 2d. As shown schematically in Figure 3b, the flat electrode is chosen to be the WE, while the sharp-tip electrode is assigned to be the QR/CE. The nanogap is connected in series with an external ballast resistor to provide self-termination as developed by Boussaad *et al.*[22] The applied potential, V_0, is then divided into a potential dropped across nanogap, V_{sample}, and that across the external resistor, V_{ext}, and the effective voltage across the sample is given by

$$V_{sample}(t) = \frac{R_{sample}(t)}{R_{sample}(t) + R_{ext}} V_0 \quad (2)$$

where $R_{sample}(t)$ initially is the gap resistance, then becomes the ASJ resistance upon junction formation. Initially, R_{sample} is very large because conduction across the nanogap occurs through the electrolyte solution, and $R_{sample} \gg R_{ext}$, so $V_{sample} \sim V_0$. As the ASJ forms, R_{sample} drops precipitously into the range $R_{sample} \sim (1/nG_0)$, which, under typical conditions, is comparable to R_{ext}, meaning that V_{sample} is much smaller after junction formation. The conductance of the ASJ can be easily calculated, in units of G_0, from the voltage and current acquired by the potentiostat and the value of the external ballast resistor

$$G(G_0) = \frac{h}{2e^2\left[\frac{V_0}{i} - R_{ext}\right]} \quad (3)$$

In contrast to the work of Boussaad *et al.*, which used one electrode as a source for deposition on the other, the ASJ fabricated here uses a second metal, Ag, to minimize damage to the Au nanoband electrodes and render the devices reusable.

In the nanoscale WE CV experiments described above, the potential for Ag deposition varies with the nature and history of the electrode. Thus, rather than attempting to determine a well-defined voltage for Ag electrodeposition, sequential increasingly cathodic voltage pulses (initially 0 to −0.1 V to 0, with the cathodic excursion increasing in increments of 0.05 V to a final pulse magnitude of −0.8 V) in 10 μM Ag_2SO_4 + 0.1 M K_2SO_4 solution were used. Figure 6 shows a typical conductance−time trace of an ASJ fabrication by this strategy. Deposition is observed at a cathodic pulse magnitude of $V_0 = -0.65$ V, so at potentials more anodic than −0.65 V, the current response is limited by ionic conductance, yielding $G \sim 0$. When the applied potential reaches a sufficiently cathodic value, the conductance jumps to 50−60 G_0, as the two electrodes are connected with an overgrown Ag junction. The strong electric field in the vicinity of the sharp tip is expected to force the junction to be highly directional from one electrode to the other. Within a few seconds, however, the junction conductance drops to a low and stable value, in this experiment $G \sim 0.5\ G_0$ (right inset of Figure 6), a result that can be understood in terms of the initially formed Ag junction self-thinning by dissolving back into solution, as V_{sample} is lowered upon making contact and completing the ASJ. Controlling the bulk solution Ag^+ concentration controls the self-thinning process and regulates the final ASJ size and conductance, as shown in Figure 6. Using this fabrication protocol, ASJs can be fabricated with a repeatable temporal evolution in which a thick junction forms initially, followed by a self-thinning process to eventually produce a stabilized ASJ.

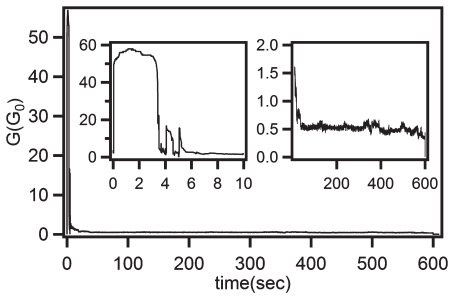

Figure 6. Conductance−time trace of a Au−Ag−Au bimetallic ASJ fabricated by electric field focused overgrowth and self-thinning, using $V_0 = -0.65$ V, $R_{ext} = 3.98$ kΩ. (Left inset) Expanded view of the initial 10 s showing overgrowth and spontaneous self-thinning. (Right inset) Expanded view showing that the junction stabilizes at $G \sim 0.5\ G_0$ for hundreds of seconds.

Mechanically Stable ASJs under Flow and Fluid Switching. ASJs fabricated by electrochemical methods are good candidates for chemical sensing because their small size enhances the sensitivity to molecular adsorption. Several groups have used ASJs fabricated by electrochemical methods for detection of adsorbed molecules.[6,17] However, mechanical stability of ASJs remains a concern because at their narrowest point ASJs consist of only a few atoms. Indeed, removing the fabrication solution and switching to analyte solution must be accomplished by carefully executed manual manipulations. There are several literature reports utilizing microfluidic channels to introduce and switch different solutions, but not in the presence of stable ASJs.[24,26] To address this issue, the usual preference for small dimension channels is discarded here in favor of a PDMS fluidic channel of 1 mm × 0.5 mm cross section for transport of solution to the ASJ. The linear flow velocity in such a large channel is ≥100 times slower than a typical microchannel at the same volume flow rate. Figure 7 shows the result of ASJ formation in flowing ($F_V = 0.1$ mL h^{-1}) 10 μM Ag_2SO_4/0.1 M K_2SO_4 solution. As expected, the initial overgrown junction forms rapidly, and the conductance rises from 0 to 35 G_0 within a few seconds at $V_0 = -0.4$ V *versus* Au film QR/CE. The conductance then decays over a period of ~20 s before stabilizing at $G \sim 2\ G_0$ for almost 600 s (Figure 7, inset 2). Clearly, the ASJ can be very stable in the presence of slow fluid flow as seen in the figure.

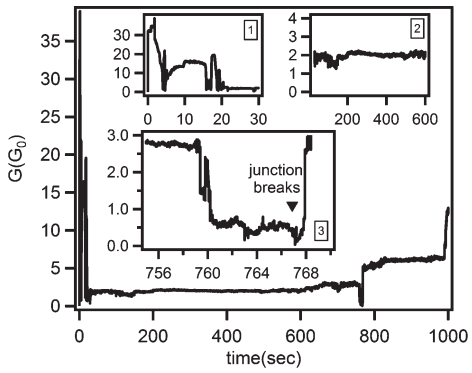

Figure 7. Conductance–time trace of ASJ formation in 10 μM Ag_2SO_4/0.1 M K_2SO_4 solution under flow (0.10 mL h^{-1}) at $V_0 = -0.4$ V and $R_{ext} = 15.86$ kΩ. (Inset 1) Expanded time trace of initial overgrown junction formation when V_0 is applied. (Inset 2) Expanded view of junction conductance stable at $\sim 2\ G_0$. (Inset 3) Expanded view of junction breaking to atomic size gap (767 s) prior to spontaneous redeposition to a stable 6 G_0 junction.

Even when instabilities occur, as observed in the period of ~760–770 s, when the junction narrows to $G \sim 0.5\ G_0$, eventually breaking (Figure 7, inset 3), V_{sample} transitions back to a large value, reinitiating Ag deposition, which quickly connects the two electrodes again (~768 s).

To further investigate how fluid switching affects the stability of ASJs, an experiment was performed while the electrolyte solution was switched directly to DI water or to air then to DI water. The upstream tubing connecting the PDMS-based fluidic channel to the pump was prefilled with different sectors of media and the conductance–time trace observed during switching from electrolyte solution to water, as demonstrated in Figure 8a. At ~160 s, a conductance transient is observed when solution changeover occurs; however, when the ASJ is immersed in water again, it immediately stabilizes. Ag is stable in DI water because the lack of electrolyte imposes a large overpotential for Ag dissolution. Figure 8b shows an ASJ going through a transition from electrolyte solution to air then to DI water. At 200 s, the solution is changed to air, and a large conductance transient is followed by the conductance stabilizing near 3 G_0. When DI water is reintroduced at ~600 s, the conductance immediately jumps back to a value near the initial conductance (before introduction of air). The large difference in steady-state conductance for a relatively stable ASJ when exposed to air *versus* water can be attributed to the dielectric boundary layer effect,[33] and the large fluctuation in conductance at switchover is likely due to differences in surface tension.

Fractional Conductance in Electrochemically Fabricated ASJs. Fractional conductance has been observed in ASJs fabricated by both mechanical[34–36] and electrochemical methods.[23,24] Tao and co-workers assign fractional conductance to an adsorbate effect that induces scattering in ballistic transport and changes the atomic configuration

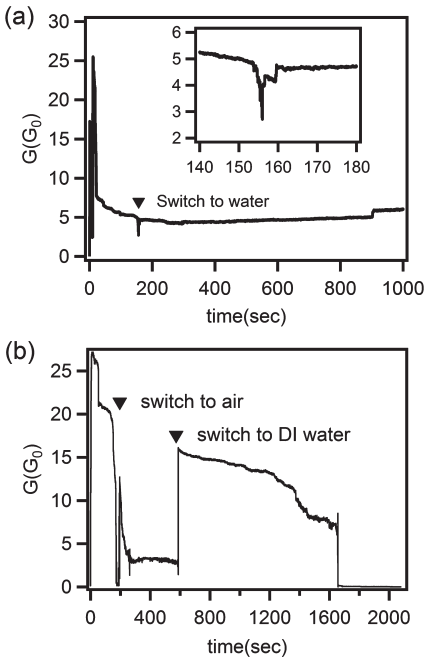

Figure 8. (a) Conductance–time trace of ASJ during switching from electrolyte solution to DI water at $V_0 = -0.75$ V, $R_{ext} = 16$ kΩ. (Inset) Expanded view showing the conductance transient due to solution exchange. (b) Conductance–time trace of ASJ during switching from electrolyte solution to air to DI water at $V_0 = -0.75$ V, $R_{ext} = 16$ kΩ.

of the junctions.[6,19] In addition, the electrochemical potential of the junction can be controlled to determine the effects of double layer charging, anion adsorption, and potential-induced surface stress.[7,34] Several groups have shown both experimentally[35–37] and theoretically[38,39] that ASJs dimerize in the presence of hydrogen and exhibit fractional conductance. In the ASJ fabrication experiments conducted here, fractional conductance is frequently observed, but the current experiments are carried out in the absence of specific adsorbates and in the potential range where hydrogen evolution is not expected.

de Heer *et al.* used high-speed precision measurements to show that nanojunctions can be composed of several quantized ASJs in series.[40] Evidence consistent with this interpretation has also been found in the ASJ fabrication data obtained here. Figure 9a is a conductance–time trace of a junction fluctuating within the range $G < 5\ G_0$. The histogram of the frequencies with which individual conductance states are observed (Figure 9a, inset) shows several distinct peaks. Two prominent peaks are observed near 0.5 and 0.67 G_0, fractional values which, according to de Heer's model, result from a 1 G_0 ASJ in series with another 1 G_0 junction, to give 0.5 G_0, or with a 2 G_0 ASJ, to give 0.67 G_0. Several smaller peaks can also be assigned to binary combinations of small integer G_0 ASJs, including 0.83 G_0 (=1 G_0 + 5 G_0), ~1 G_0; 1.28 G_0 (~2 G_0 + 4 G_0); 1.4 G_0 (~2 G_0 + 5 G_0); and 1.7 G_0 (~3 G_0 + 4 G_0). In this model, the conductance trace can display complicated behavior

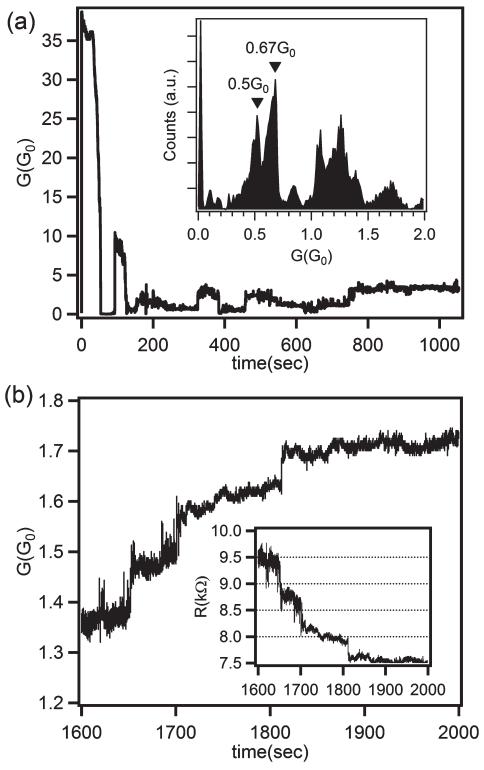

Figure 9. (a) Conductance–time trace of a junction showing conductance fluctuations in the range $G < 5G_0$. (Inset) Conductance histogram containing fractional conductance peaks. (b) Conductance–time trace of an ASJ showing fractional G_0 step increments. (Inset) Same data plotted as a resistance change.

if more than two ASJs are in series in a sample. In Figure 9b, several discrete conductance states are observed at fractional G_0 values. A perfect single ASJ system would be expected to show a 1 G_0 change between each discrete conductance state corresponding to the different quantum modes of electron wave propagation. However, in the ASJs-in-series model, the 1 G_0 difference between discrete states of one particular ASJ is suppressed into fractional changes because the conductance is not additive in a series circuit. Therefore, to decipher how the observed fractional G_0 states correspond to different quantum states of one member of multiple ASJs in series, the resistance *versus* time trace is plotted (Figure 9b, inset) because series resistance is additive. For example, the simplest possible configuration that can explain the conductance at $t = 1600$ s, $G \sim 4/3\ G_0$, is composed of 2 and 4 G_0 conductors in series. The resistance drop between the first two states is ~650 Ω, which matches the resistance difference (645 Ω) of a state change from 4 to 5 G_0 of the second ASJ; the following drop is ~400 Ω, agreeing with the resistance change from 5 to 6 G_0 (430 Ω), and in the final drop, the resistance changes ~300 Ω, which corresponds to the resistance change of 6 to 7 G_0 (307 Ω). Thus, the results obtained here are consistent with a simple ASJs-in-series model in which the discrete fractional G_0 conductance states in the range of 1–2 G_0 result from single quantum G_0 transitions of one ASJ in a series ASJ arrangement.

According to theory, ballistic transport occurs when the length of the junction is much smaller than the mean free path of an electron in the metal. The mean free path of electrons in bulk Ag at 300 K is 52 nm[41] and decreases with the size of the wire. The gap between two Au electrodes, which defines the largest extent of a Ag nanowire, is 100–150 nm, which is larger than the mean free path, which means that the physical presence of several quantum ASJs in series within a single nanowire is at least plausible.

CONCLUSIONS

A new electrochemical method has been developed to fabricate Au–Ag–Au bimetallic ASJs, by sequential overgrowth and self-thinning in the presence of a judiciously chosen amount of aqueous Ag^+ at a tip and anvil Au nanogap. The self-limiting growth strategy described here produces mechanically robust functional structures in high (approaching unity) yield and great stability. Several elements of the design are crucial to its success. The Au electrodes are designed into tip and anvil shapes with a 100–150 nm separation in order to generate a strong, directional electric field when potential is applied. In the initial deposition, Ag is overgrown to produce a high conductance nanowire, but an external resistor in series with the ASJ controls the potential drop across the ASJ and thus the driving potential for self-thinning. Compared to previous ASJ fabrication strategies developed in this laboratory, the near unity yield compares favorably with direct electrodeposition without self-thinning[17] (yield ~1%) and the open WE approach[12] (yield ~10%). The chemical potential of the solution, which is primarily determined by the bulk Ag^+ concentration, and current-induced electromigration are the two biggest factors which affect the self-dissolution process and the stability of fabricated ASJ.

A millimeter-scale PDMS fluidic channel is coupled with the sample as a flow cell, with the large dimensions of the channel greatly reducing the linear flow velocity. As fabricated, the ASJs show extraordinary mechanical stability, both in flow and during solution switching. The ASJs are especially stable when the electrolyte solution is switched to DI water because the lack of electrolyte ensures a high overpotential for reconstruction of the ASJ by charge-transfer reactions. Thus, during phase change, the principal challenge to structural integrity of the ASJ arises from changes in surface tension. In addition, fractional conductance states are observed, which most likely result from the presence of two or more quantized ASJs in series between the two microscale Au electrodes. The conductance histogram and continuous step change analysis support this interpretation. In summary, using this self-limiting fabrication method, highly mechanically

robust Au–Ag–Au bimetallic ASJs can be repeatedly and reproducibly fabricated, and their robustness to flow and media switching shows promise for future applications in chemical and biochemical sensing.

EXPERIMENTAL SECTION

Template Preparation. Templates are fabricated through a sequence of microfabrication procedures, viz. Figure 1. First, a 100 nm thick Au microbridge, *ca.* 6 μm wide $\times$ 20 μm long, is defined by standard photolithography and lift-off techniques on an oxidized (500 nm SiO_2) Si wafer (Silicon Quest International, CA). A thin ($\sim$100 nm) layer of SiN_x is then deposited by plasma-enhanced chemical vapor deposition (PECVD) over the entire sample surface. To expose the gold contact pad, SiN_x is removed by reactive ion etching, using a Cr etch mask to protect the SiN_x in the area where the nanogap is to be fabricated. Cr is then removed using CR-4 etchant (Cyantek Corporation). Figure 2a shows a macroscopic view of the sample; the rectangular area in the middle is covered with SiN_x. The highlighted area contains the Au microbridge, which is then FIB-milled (FEI Helios NanoLab 600 dual-beam system) to form the nanogap. Two different electrode designs are used. For electrochemical characterization, two flat electrodes separated by a $\sim$3 μm gap are prepared, as shown in Figure 2b. To form ASJs, a tip and anvil design, shown in Figure 2c, is used. Typically, the distance between the end of the tip and the flat section is $\sim$100 nm. Because the top of the structure is covered with SiN_x, the side faces of the electrodes are the only areas exposed to solution in subsequent electrochemical experiments. Finally, the sample is immersed in 1:1 (v/v) aqueous HNO_3 after FIB milling.

Electrochemistry and Ag ASJ Formation. A commercial potentiostat (Gamry Instruments, Reference 600) is used in all electrochemical experiments. Cyclic voltammetry (CV) experiments are implemented in a two-electrode configuration, as shown in Figure 3a. One of the two planar electrodes is used as the working electrode (WE), and a separate 2 mm wide Au thin film serves as a quasi-reference/counter electrode (QR/CE), *cf.* Figure 2a. Macroscopic CV experiments use two thin (0.5 mm) Au wires as WE and QR/CE. All electrochemical experiments are carried out in 0.1 M K_2SO_4 supporting electrolyte and different concentrations of Ag_2SO_4 (1 μM, 10 μM, 100 μM, and 1 mM) for deposition/dissolution. A fluidic channel (1 mm $\times$ 500 μm) is fabricated by casting a mixture of polydimethylsiloxane (PDMS) prepolymer and curing agent (Sylgard 184, Dow Corning) on an aluminum mold at 95 °C for 1 h. After curing, the channel is O_2-plasma-treated, aligned, and sealed on the template so that both the WE and QR/CE are confined in the channel. Solutions are introduced to the channel using a syringe pump through PVC tubing. For the CV experiments, the flow is stopped once the solutions completely fill the channel.

Au–Ag–Au bimetallic ASJs are fabricated using the tip–anvil electrode design shown schematically in Figure 3b. The potentiostat applies a constant voltage between the WE and QR/CE while simultaneously measuring current to monitor junction formation. An external resistor is placed in series with the nanogap/ASJ, forming a voltage divider and limiting current once the ASJ is formed. Different values, 2 kΩ < R_{ext} < 16 kΩ, are selected to investigate to achieve different limiting currents. ASJs are formed by galvanic reaction in an electrolyte solution containing 10 μM Ag_2SO_4 and 0.1 M K_2SO_4. ASJs are fabricated in both stationary and flowing solution conditions. To maintain ASJ's mechanical stability in flowing condition, the flow rate is set to 0.10 mL h^{-1}, with a corresponding linear velocity of $\sim$50 μm s^{-1}. The tubing connecting the PDMS channel with the syringe pump is filled with a volume of reaction solution followed by a segment of different media as a switching protocol to minimize mechanical perturbation while switching fluids.

Acknowledgment. This work was conducted with support from the National Science Foundation (NSF0807816) and the Army Corps of Engineers (W9132T-07-2-0003).

REFERENCES AND NOTES

1. Costa-Kramer, J. L.; Garcia, N.; Garcia-Mochales, P.; Serena, P. A.; Marques, M. I.; Correia, A. Conductance Quantization in Nanowires Formed between Micro and Macroscopic Metallic Electrodes. *Phys. Rev. B* **1997**, *55*, 5416–5424.
2. Brandbyge, M.; Sorensen, M. R.; Jacobsen, K. W. Conductance Eigenchannels in Nanocontacts. *Phys. Rev. B* **1997**, *56*, 14956–14959.
3. Scheer, E.; Agrait, N.; Cuevas, J. C.; Yeyati, A. L.; Ludoph, B.; Martin-Rodero, A.; Bollinger, G. R.; van Ruitenbeek, J. M.; Urbina, C. The Signature of Chemical Valence in the Electrical Conduction through a Single-Atom Contact. *Nature* **1998**, *394*, 154–157.
4. Hakkinen, H.; Barnett, R. N.; Landman, U. Gold Nanowires and Their Chemical Modifications. *J. Phys. Chem. B* **1999**, *103*, 8814–8816.
5. Rodrigues, V.; Fuhrer, T.; Ugarte, D. Signature of Atomic Structure in the Quantum Conductance of Gold Nanowires. *Phys. Rev. Lett.* **2000**, *85*, 4124–4127.
6. Bogozi, A.; Lam, O.; He, H. X.; Li, C. Z.; Tao, N. J.; Nagahara, L. A.; Amlani, I.; Tsui, R. Molecular Adsorption onto Metallic Quantum Wires. *J. Am. Chem. Soc.* **2001**, *123*, 4585–4590.
7. Xu, B. Q.; He, H. X.; Boussaad, S.; Tao, N. J. Electrochemical Properties of Atomic-Scale Metal Wires. *Electrochim. Acta* **2003**, *48*, 3085–3091.
8. Xie, F. Q.; Obermair, C.; Schimmel, T. Switching an Electrical Current with Atoms: The Reproducible Operation of a Multi-atom Relay. *Solid State Commun.* **2004**, *132*, 437–442.
9. Umeno, A.; Hirakawa, K. Fabrication of Atomic-Scale Gold Junctions by Electrochemical Plating Using a Common Medical Liquid. *Appl. Phys. Lett.* **2005**, *86*, 143103.
10. Li, X. L.; Hua, S. Z.; Chopra, H. D.; Tao, N. J. Formation of Atomic Point Contacts and Molecular Junctions with a Combined Mechanical Break Junction and Electrodeposition Method. *Micro Nano Lett.* **2006**, *1*, 83–88.
11. Neel, N.; Kroger, J.; Limot, L.; Palotas, K.; Hofer, W. A.; Berndt, R. Conductance and Kondo Effect in a Controlled Single-Atom Contact. *Phys. Rev. Lett.* **2007**, *98*, 016801.
12. Shi, P.; Bohn, P. W. Stable Atom-Scale Junctions on Silicon Fabricated by Kinetically Controlled Electrochemical Deposition and Dissolution. *ACS Nano* **2008**, *2*, 1581–1588.
13. Tao, N. J. Electrochemical Fabrication of Metallic Quantum Wires. *J. Chem. Educ.* **2005**, *82*, 720–726.
14. Agrait, N.; Yeyati, A. L.; van Ruitenbeek, J. M. Quantum Properties of Atomic-Sized Conductors. *Phys. Rep.* **2003**, *377*, 81–279.
15. Park, J.; Pasupathy, A. N.; Goldsmith, J. I.; Chang, C.; Yaish, Y.; Petta, J. R.; Rinkoski, M.; Sethna, J. P.; Abruna, H. D.; McEuen, P. L.; Ralph, D. C. Coulomb Blockade and the Kondo Effect in Single-Atom Transistors. *Nature* **2002**, *417*, 722–725.
16. Xie, F. Q.; Huser, F.; Pauly, F.; Obermair, C.; Schon, G.; Schimmel, T. Conductance of Atomic-Scale Pb Contacts in an Electrochemical Environment. *Phys. Rev. B* **2010**, *82*, 075417.
17. Castle, P. J.; Bohn, P. W. Interfacial Scattering at Electrochemically Fabricated Atom-Scale Junctions between Thin Gold Film Electrodes in a Microfluidic Channel. *Anal. Chem.* **2005**, *77*, 243–249.
18. Li, C. Z.; He, H. X.; Bogozi, A.; Bunch, J. S.; Tao, N. J. Molecular Detection Based on Conductance Quantization of Nanowires. *Appl. Phys. Lett.* **2000**, *76*, 1333–1335.
19. Li, C. Z.; Sha, H.; Tao, N. J. Adsorbate Effect on Conductance Quantization in Metallic Nanowires. *Phys. Rev. B* **1998**, *58*, 6775–6778.
20. Tsutsui, M.; Shoji, K.; Taniguchi, M.; Kawai, T. Formation and Self-Breaking Mechanism of Stable Atom-Sized Junctions. *Nano Lett.* **2008**, *8*, 345–349.

21. Xu, B. Q.; Tao, N. J. J. Measurement of Single-Molecule Resistance by Repeated Formation of Molecular Junctions. *Science* **2003**, *301*, 1221–1223.
22. Boussaad, S.; Tao, N. J. Atom-Size Gaps and Contacts between Electrodes Fabricated with a Self-Terminated Electrochemical Method. *Appl. Phys. Lett.* **2002**, *80*, 2398–2400.
23. Li, J. Z.; Kanzaki, T.; Murakoshi, K.; Nakato, Y. Metal-Dependent Conductance Quantization of Nanocontacts in Solution. *Appl. Phys. Lett.* **2002**, *81*, 123–125.
24. Shi, P.; Bohn, P. W. Electrochemical Control of Stability and Restructuring Dynamics in Au−Ag−Au and Au−Cu−Au Bimetallic Atom-Scale Junctions. *ACS Nano* **2010**, *4*, 2946–2954.
25. Meszaros, G.; Kronholz, S.; Karthauser, S.; Mayer, D.; Wandlowski, T. Electrochemical Fabrication and Characterization of Nanocontacts and nm-Sized Gaps. *Appl. Phys. A: Mater. Sci. Process.* **2007**, *87*, 569–575.
26. Lunco Popa, P.; Dalmas, G.; Faramarzi, V.; Dayen, J. F.; Majjad, H.; Kemp, N. T.; Doudin, B. Heteronanojunctions with Atomic Size Control Using a Lab-on-Chip Electrochemical Approach with Integrated Microfluidics. *Nanotechnology* **2011**, *22*, 215302.
27. Morpurgo, A. F.; Marcus, C. M.; Robinson, D. B. Controlled Fabrication of Metallic Electrodes with Atomic Separation. *Appl. Phys. Lett.* **1999**, *74*, 2084–2086.
28. Xie, F. Q.; Maul, R.; Brendelberger, S.; Obermair, C.; Starikov, E. B.; Wenzel, W.; Schon, G.; Schimmel, T. Preselectable Integer Quantum Conductance of Electrochemically Fabricated Silver Point Contacts. *Appl. Phys. Lett.* **2008**, *93*, 043103.
29. Wibbeler, J.; Pfeifer, G.; Hietschold, M. Parasitic Charging of Dielectric Surfaces in Capacitive Microelectromechanical Systems (MEMS). *Sens. Actuators, A* **1998**, *71*, 74–80.
30. Koutsoureli, M.; Tavassolian, N.; Papaioannou, G.; Papapolymerou, J. Dielectric Charging in Capacitive Microelectromechanical System Switches with Silicon Nitride. *Appl. Phys. Lett.* **2011**, *98*, 093505.
31. Rogers, L. B.; Krause, D. P.; Griess, J. C.; Ehrlinger, D. B. The Electrodeposition Behavior of Traces of Silver. *J. Electrochem. Soc.* **1949**, *95*, 33–46.
32. Chen, C. H.; Vesecky, S. M.; Gewirth, A. A. *In Situ* Atomic Force Microscopy of Underpotential Deposition of Ag on Au(111). *J. Am. Chem. Soc.* **1992**, *114*, 451–458.
33. Jena, D.; Konar, A. Enhancement of Carrier Mobility in Semiconductor Nanostructures by Dielectric Engineering. *Phys. Rev. Lett.* **2007**, *98*, 136805.
34. Xu, B. Q.; He, H. X.; Tao, N. J. Controlling the Conductance of Atomically Thin Metal Wires with Electrochemical Potential. *J. Am. Chem. Soc.* **2002**, *124*, 13568–13575.
35. Csonka, S.; Halbritter, A.; Mihaly, G.; Jurdik, E.; Shklyarevskii, O. I.; Speller, S.; van Kempen, H. Fractional Conductance in Hydrogen-Embedded Gold Nanowires. *Phys. Rev. Lett.* **2003**, *90*, 116803.
36. Kiguchi, M.; Konishi, T.; Miura, S.; Murakoshi, K. The Effect of Hydrogen Evolution Reaction on Conductance Quantization of Au, Ag, Cu Nanocontacts. *Nanotechnology* **2007**, *18*, 424011.
37. Kiguchi, M.; Konishi, T.; Hasegawa, K.; Shidara, S.; Murakoshi, K. Three Reversible States Controlled on a Gold Monoatomic Contact by the Electrochemical Potential. *Phys. Rev. B* **2008**, *77*, 245421.
38. Santos, E.; Quaino, P.; Soldano, G.; Schmickler, W. Electrochemical Reactivity and Fractional Conductance of Nanowires. *Electrochem. Commun.* **2009**, *11*, 1764–1767.
39. Barnett, R. N.; Hakkinen, H.; Scherbakov, A. G.; Landman, U. Hydrogen Welding and Hydrogen Switches in a Monatomic Gold Nanowire. *Nano Lett.* **2004**, *4*, 1845–1852.
40. deHeer, W. A.; Frank, S.; Ugarte, D. Fractional Quantum Conductance in Gold Nanowires. *Z. Phys. B: Condens. Matter* **1997**, *104*, 469–473.
41. Reynolds, F. W.; Stilwell, G. R. Mean Free Paths of Electrons in Evaporated Metal Films. *Phys. Rev.* **1952**, *88*, 418–419.